Molecular Therapy
Methods & Clinical Development
Original Article

Targeted spiral ganglion neuron degeneration in parvalbumin-Cre neonatal mice

Nhi V. Nguyen,[1] Joshua S. Lin,[1] Miti J. Parikh,[2] Raffaello M. Cutri,[3] and Seiji B. Shibata[1]

[1]Caruso Department of Otolaryngology-Head and Neck Surgery, University of Southern California, Los Angeles, CA 90033, USA; [2]Keck School of Medicine, University of Southern California, Los Angeles, CA 90033, USA; [3]Department of Otolaryngology-Head and Neck Surgery, Cedars Sinai Medical Center, Los Angeles, CA 90048, USA

The spiral ganglion neurons (SGNs) are the primary afferent neurons in the cochlea; damage to the SGNs leads to irreversible hearing impairment. Mouse models that allow selective SGN degeneration while sparing other cell types in the cochlea are lacking. Here, we investigated a genetic ablation method of the SGN using a Cre-responsive adeno-associated virus (AAV) vector expressing diphtheria toxin subunit-A (DTA). We microinjected AAV2-retro-FLEX-DTA-mCherry driven by the EF1a or hSYN promoter in neonatal parvalbumin-Cre (PV^{Cre}) and wild-type strains via the posterior semicircular canal. Apoptotic markers were observed in the degenerating SGNs as early as 3 days. After 1 week, we assessed the SGN cell density, revealing an average degeneration of 60% for AAV-DTA driven by the EF1a promoter and 61% for that driven by the hSYN promoter. By 1 month, injected ears demonstrated a nearly complete loss of SGN, while hair cell morphology was intact. The auditory brain stem response result showed significantly elevated threshold shifts at 1 month, while the distortion-product otoacoustic emissions function remained intact. Furthermore, we show that our method did not effectively ablate SGN in adult PV^{Cre} mice. We generated a neonatal mouse model with primary SGN degeneration in PV^{Cre} mice, mimicking auditory neuropathy phenotype using an AAV Cre-dependent expression of DTA.

INTRODUCTION

Hearing loss is a public health issue, affecting 30 million people in the United States.[1] Current treatments for sensorineural hearing loss (SNHL) are limited to hearing aids and cochlear implants, a neuroprosthesis that bypasses hair cells (HCs) to stimulate spiral ganglion neurons (SGNs). These interventions, while effective, do not restore natural hearing, spurring the need for further research and development of novel therapeutics for HC and SGN regeneration and protection.

SGNs are the primary afferent auditory neurons in the mammalian inner ear that connect the mechanosensory HCs to the cochlear nucleus to transmit acoustic signals. SGNs are bipolar neurons divided grossly into two subtypes; type I neurons connect multiple neurites to a single inner HC (IHC) and type II neurites connect to multiple outer HCs (OHCs). The type I neurons that comprise 95% of the SGN population can be further characterized as type Ia, Ib, and Ic based on functionality during development. Type II neurons make up about 5% of the neurons and are thought to play a significant role in auditory processing.[2,3]

Previously, it was believed that SGN loss occurred secondary to HC damage; however, we now know that primary cochlear nerve synaptopathy and SGN loss can occur without HC damage due to multiple causes, including noise, aging, and genetics.[4–8] This afferent nerve loss can underlie auditory neuropathy (AN) which is characterized as having absent auditory brain stem thresholds but normal cochlear microphonics and otoacoustic emission. AN is seen in approximately 2%–10% of hearing loss patients, and the degree of hearing loss ranges from moderate to profound.[9] SGNs lack intrinsic regenerative capacity; thus, auditory nerve injury or destruction result in permanent SNHL. The damage or loss of SGNs hinders the effectiveness of the cochlear implant, which depends on the health of the nerve.[10] Thus, there is a critical need to develop novel treatments for AN; however, animal models mimicking AN are lacking.

Multiple studies have sought to develop models of AN through ototoxic drugs (e.g., ouabain, carboplatin, aminoglycosides, glutamate-induced excitotoxicity) and surgical nerve amputation and compression.[11–14] While these methods are effective, off-target side effects of ototoxic drugs and surgical manipulation can lead to variable results and, at times, may be lethal. Efforts have been made to create a more reliable model through genetic conditional ablation. Recent studies have attempted to create a transgenic mice line to ablate SGNs, specifically crossing a Cre-inducible diphtheria toxin receptor (DTR) mouse line with a mouse line containing Cre recombinase in SGN-specific promoter. For example, adult *Bhlhb5* mice with SGN-selective Cre expression crossed with the DTR mice induced 30%–40% SGN loss 7 days after DT injection without damaging the HCs.[15] In another study, mice with *Nefl* gene Cre were bred with DTR mice. Since *Nefl* gene encodes neurofilament light chain, which is exclusively expressed in the cochlear SGNs, DT injection to these mice at postnatal day 7 (P7) induced approximately 58% of selective

Received 15 September 2024; accepted 27 February 2025;
https://doi.org/10.1016/j.omtm.2025.101440.

Correspondence: Seiji B. Shibata, MD, PhD, Caruso Department of Otolaryngology-Head and Neck Surgery, University of Southern California, Los Angeles, CA 90033, USA.
E-mail: seiji.shibata@med.usc.edu

SGN damage by 28 days.[16] However, the ablation of SGN in the early neonatal period (<P14) using DTR mice has not been reported.

Here, we characterized a neonatal mouse model of AN using a viral mediated Cre-responsive flip-excision (FLEX) switch system to express DT subunit A (DTA), which is the cleaved DT toxin without the cell entry ligand, DT subunit B. DTA inhibits protein synthesis that leads to cellular apoptosis through its inactivation of the eukaryotic elongation factor 2.[17,18] Rodents do not express diphtheria receptors; therefore, DTA induces apoptosis of the targeted cell without affecting the neighboring cells.[19] The FLEX switch system utilizes two-site-specific recombination, which leads to translocation and inversion of the payload in the presence of Cre recombinase.[20,21] We packaged this construct in an adeno-associated virus (AAV)-retro serotype that has neuronal tropism in the cochlea without transfecting the HCs. We delivered AAV-retro harboring FLEX-DTA-mCherry driven by either the ubiquitous EF1a promoter (AAV-eF1a-DTA) or the neuronal hSYN (AAV-hSYN-DTA) promoter into the cochlea of P2 parvalbumin-Cre knockin mice (PV^{Cre}) in which Cre recombinase is widely expressed in the parvalbumin-expressing SGNs and HCs in neonates and adults.[22,23] We demonstrate apoptosis of the SGN as early as 3 days post-injection (dpi) followed by robust SGN loss of up to 60%–61% in all turns by 7 dpi, regardless of promoter types. Likewise, we observed a near-total SGN loss with absent auditory brain stem response (ABR) thresholds after 28 dpi, while HC morphology and distortion product otoacoustic emissions (DPOAE) thresholds remained grossly intact. Furthermore, we observed significant neuronal damage in the non-injected contralateral ear SGNs and vestibular ganglion by 1 month. However, AAV-DTA injection did not effectively lead to significant SGN ablation in the adult PV^{Cre}. This model mimics a severe form of AN in humans and allows us to reliably ablate SGNs in neonatal mice.

RESULTS

AAV-retro serotype transfects SGNs with high efficiency

We investigated the transduction profile of AAV2-retro serotype to assess for neuronal tropism in the inner ear. AAV2-retro serotype is a designer AAV variant shown to allow neuronal tropism and efficient retrograde access to nerve fibers.[24] AAV2-retro-cytomegalovirus (CMV)-GFP vector was injected into the cochlea via the posterior semicircular canal (PSCC) in P2 mice. Imaging of the mid-modiolar cross-section collected on 7 dpi demonstrates robust GFP localization to the SGN cells in Rosenthal's canal throughout the cochlear duct (Figure 1A). GFP signals are appreciated along the nerve fibers; however, the phalloidin-positive HCs were not transduced (Figure 1A, inset). Minimal ectopic GFP distribution in the lateral wall and stria vascularis was appreciated. These observations indicate that the AAV2-retro serotype has high SGN tropism without HC transduction in the neonatal cochlea.

AAV2-retro-FLEX-DTA-mCherry express DTA in PV^{Cre+} cells

We packaged the FLEX-DTA-mCherry construct with an AAV2-retro (AAV-DTA) capsid (Figure 1B). The AAV contains open reading frames flanked by oppositely positioned Cre recognition sites loxP and lox2272. In the presence of Cre recombinase, the FLEX-DTA-mCherry construct activates the transgene by mediating the inversion of the DTA sequence from the anti-sense to the sense direction, activating the transgene. Successful transduction of AAV-DTA thus allows for DTA expression in the presence of Cre recombinase. Transduced cells without Cre recombinase express mCherry alone, allowing Cre-dependent expression of DTA.[25,26] We tested the AAV-DTA in P1–P2 wild-type (WT) mice and PV^{Cre} mice. Parvalbumin is an acidic and cystolic Ca^{2+} binding protein, a well-known neuronal marker in the CNS, which is also expressed in the HCs and SGNs in the cochlea.[22,23,27,28] Control WT and PV^{Cre} mice were injected with AAV-DTA via the PSCC at P2. As early as 3 dpi, we observed expression of mCherry protein in the SGNs in the WT mice (Figure 1C, WT). However, mCherry expression was not identified in PV^{Cre} mice SGNs; instead, there were fewer and slightly deformed SG cells (Figure 1C, PV^{Cre}). In summary, AAV-DTA allows targeted expression of transgenes in a Cre-dependent manner in the SGNs alone.

AAV-DTA induces apoptosis of SGN

We sought to investigate whether the AAV-DTA-induced SGN death followed the process of apoptosis in the PV^{Cre} mice. We thus stained cochlear mid-modiolar sections with apoptotic markers: cleaved caspase-3 and cytochrome *c*. In WT injected at P2 and examined at P9, cleaved caspase-3 and release of cytochrome *c* were not observed. Conversely, we observed increased activation of caspase-3 in the cytoplasm of SG cells at 3 and 7 dpi, suggestive of apoptosis of the SGNs (Figure 2A). Intracellular cytochrome *c* was uniformly expressed in the WT. In 3-dpi mice, cytochrome *c* is released in the misshaped and shrunk cytoplasm of SGN in PV^{Cre} mice; the number of SGN cells is noticeably less in 7 dpi mice (Figure 2B). Our findings are indicative that AAV-DTA-induced SGN ablation follows a regulated apoptotic event.

AAV-DTA injection leads to rapid and significant SGN degeneration

To validate the expression of Cre recombinase in the inner ear, we crossed a PV^{Cre} mouse strain with an Ai9 tdTomato Cre reporter mouse strain to create heterozygous Td/PV^{Cre}. In the Td/PV^{Cre} mouse ears, there was strong tdTomato expression localized to the SGNs and HCs, consistent with previous literature.[29] In the control section, we observed $TUJ1^{+}$ neuronal soma enclosed in tdTomato signal with a 100% colocalization, confirming the presence of Cre recombinase in SGNs in Rosenthal's canal throughout the apex, middle, and basal turn of the cochlea (Figure 3A).

The promoter strength and type influence AAV-mediated gene transfer transcription level and cell selectivity.[30] We investigated how the strong ubiquitous EF1a promoter differs from the moderate and neuron-specific hSYN promoter in transducing SGNs and promoting cell death. Vectors were injected into neonatal Td/PV^{Cre} or control Td mice at P2; cochleae were harvested at 7 dpi. We then quantified the SGN density in Td/PV^{Cre} via cochlear cryosections. SGN densities of control Td mice injected with AAV-EF1a-DTA were 3,448 ± 725 neurons/10^6 μm^2 (apex), 3,346 ± 153 neurons/10^6 μm^2 (middle), and

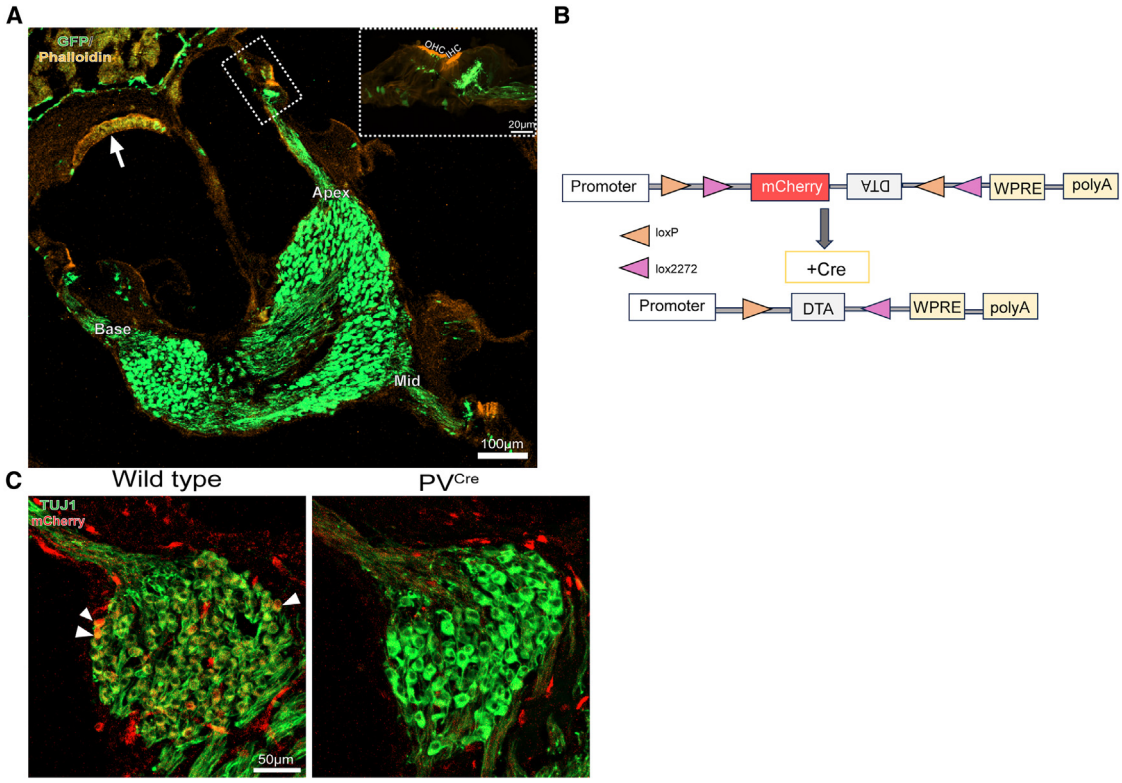

Figure 1. AAV2-retro-CMV-EGFP leads to robust SGN transduction without transducing HCs

(A) Representative low-magnification (10×) image of the cochlear mid-modiolar cross-section 7 dpi after AAV2-retro-CMV-EGFP injection. The insert demonstrates a magnified view (63×) of the organ of Corti in the dotted box. GFP is expressed in neurites but not in phalloidin-positive hair cells (HCs). GFP expression is observed in the stria vascularis (white arrow) and in the lateral wall. Of note, cochleae were stained for phalloidin alone. (B) Schematic of FLEX-DTA-mCherry plasmid, which was cloned into AAV2-retro capsid and driven under EF1a or hSYN promoter. (C) Images of representative cryosection of WT and PV^{Cre}, demonstrating the Rosenthal's canal of the basal turn of cochlea on 3 dpi following injection of AAV-DTA. Cochleae were stained for TUJ1. White arrowheads point to colocalization of mCherry and TUJ1 in the SGN in WT mice, which is not observed in PV^{Cre} mice.

3,720 ± 302 neurons/10^6 μm^2 (base), respectively (Figure 3A). The SGN densities of Td/PV^{Cre} mice injected with AAV-EF1a-DTA were 1,676 ± 225 neurons/10^6 μm^2 (apex), 1,467 ± 191 neurons/10^6 μm^2 (middle), and 1,383 ± 343 neurons/10^6 μm^2 (base), respectively (Figure 3C). The SGN densities of Td/PV^{Cre} mice injected with AAV-hSYN-DTA were 1,893 ± 119 neurons/10^6 μm^2 (apex), 1,744 ± 301 neurons/10^6 μm^2 (middle), and 1,216 ± 232 neurons/10^6 μm^2 (base) (Figure 3B). The SGN densities of Td/PV^{Cre} mice injected with AAV-EF1a-DTA were 1,676 ± 225 neurons/10^6 μm^2 (apex), 1,467 ± 191 neurons/10^6 μm^2 (middle), and 1,383 ± 343 neurons/10^6 μm^2 (base), respectively (Figure 3C). Compared to the injected control Td mice, AAV-EF1a-DTA and AAV-hSYN-DTA injected Td/PV^{Cre} neonates demonstrated an average SGN loss of 60% and 61%, respectively (Figure 3D). No statistically significant difference was observed between Td/PV^{Cre} mice injected with AAV-EF1a-DTA or AAV-hSYN-DTA (Figures 3B–3D, $p > 0.005$) in all three cochlear turns. These observations indicate that the efficiency of AAV-DTA-induced SGN cell death is not promoter dependent, and both strong ubiquitous EF1a and moderate neuron-specific hSYN promoters lead to rapid and significant SGN cell death.

Progressive SGN degeneration following AAV-DTA injection

We analyzed the AAV-hSYN-DTA-injected mice at 28 dpi from injection. We used cochlear tissue from Td/PV^{Cre} mice to accurately account for the neurons expressing Cre recombinase. In the developing mouse cochlear nerve, nerve refinement with nerve pruning and retraction occurs during the first postnatal weeks before hearing.[31] We therefore assessed age-matched control Td mice 28 days from injection. In the control Td mice, SGN densities at P30 were 3,388 ± 245 neurons/10^6 μm^2 (apex), 3,675 ± 207 neurons/10^6 μm^2 (middle), and 3,936 ± 164 neurons/10^6 μm^2 (base). We found that the cell density at P30 remained relatively similar to P9, indicating that the age of the mice is not a contributing factor to SGN loss.

At 28 dpi, we observed a near-complete loss of 95%–98% of the SGN population in the injected left ear. In addition, the non-injected contralateral right ear demonstrated a similar degeneration pattern of 92%–94% of the SGN population, suggestive of viral spread during injection. The morphology of the few surviving SGNs was smaller and disfigured compared to the control. Hence, we demonstrate the

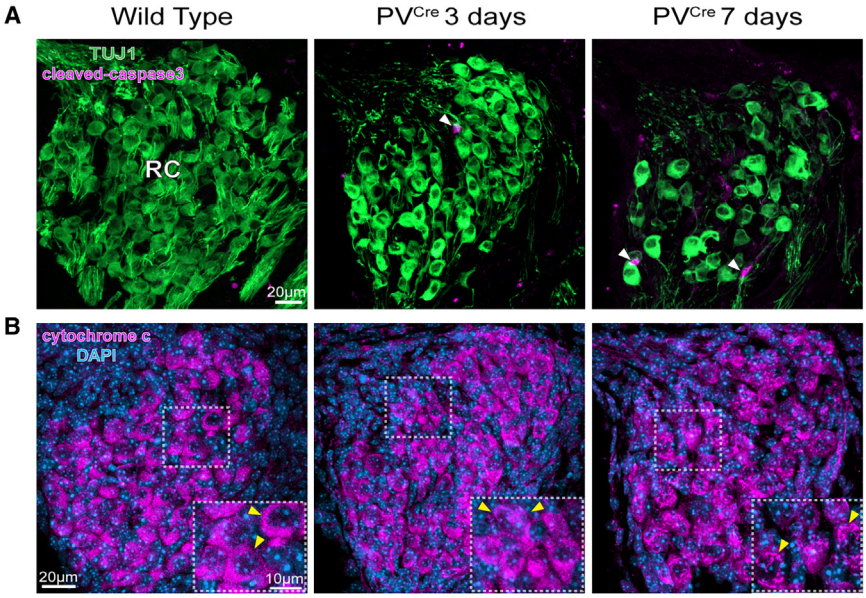

Figure 2. AAV-DTA-induced apoptosis of SGN cells
(A) The injected WT control (7 dpi) retains a healthy population of SGN in the Rosenthal's canal (RC) with negligible expression of cleaved caspase-3. Cleaved caspase-3 expression (white arrowheads) is upregulated in PV^{Cre} mice both 3 and 7 days after AAV-DTA injection. There is a noticeable degeneration of $TUJ1^{+}$ SGN by 7 days from AAV-DTA injection. (B) AAV-DTA-injected WT control mice uniformly express cytochrome *c* in the cytoplasm of SGN 7 dpi. Inserts demonstrate high magnification of cytochrome^{+} SG cells; the cytoplasm (yellow arrowheads) becomes disorganized in PV^{Cre} mice 3 and 7 dpi.

time-dependent progressive degeneration pattern following AAV-DTA injection (Figure 4A–4C).

Vestibular ganglion loss following AAV-DTA injection

We further analyzed the vestibular ganglion at 28 dpi in the left ear after AAV-hSYN-DTA injection. In the control Td mice, vestibular ganglion densities were 1,695 ± 71 neurons/10^6 μm^2 (Figures S1A–S1C). In the AAV-DTA injected Td/PV^{Cre} mice, there was a significant loss of 85% of the vestibular ganglion neuron cells, 256 ± 215 neurons/10^6 μm^2 (Figures S1B and S1C). Surprisingly, although AAV-hSYN-DTA induced significant neuronal degeneration in the vestibule, we did not observe head tilt or circling locomotion at 28 dpi.

AAV-DTA causes profound hearing loss, but HC function and morphology remain intact

We measured the auditory function with tone-burst ABR in age-matched uninjected WT control and AAV-DTA injected Td/PV^{Cre} mice 28 dpi. Td/PV^{Cre} mice demonstrated a significantly elevated threshold above 90 dB at 8, 16, 24, and 32 kHz. In contrast, DPOAE amplitude at 16 kHz was not statistically different between WT control and AAV-DTA-injected mice. Our findings indicate that while AAV-DTA-injected mice have near-complete ablation of SG cells, HC function in DPOAE amplitude is not impacted (Figures 5A and 5B). Our results demonstrate elevated ABR thresholds with an intact HC function, which is consistent with AN.

To investigate the potential off-target ototoxicity of AAV-DTA, we examined the HC survival at P30 in Td/PV^{Cre} mice. The whole-mount tissues were stained with HC-specific marker Myo7a. We demonstrate the colocalization of Myo7a with tdTomato expression. Both the IHC and OHC remained intact in all turns (Figure 6). We concluded that the AAV-DTA had limited to no off-target toxicity to the HC.

AAV-DTA injection leads to afferent nerve fiber degeneration

We next assessed the nerve fibers crossing the osseous spiral lamina (OSL) and innervating the HCs. Afferent fibers and efferent fibers from the lateral olivocochlear complex (LOC) form the inner spiral bundle (ISB) at the base of the IHC. The efferent fibers from the LOC synapse to the afferent fibers at the base of the IHC.[32] Type II afferents form the outer spiral bundle (OSB), and medial olivocochlear complex (MOC) efferent fibers send radial fibers and form terminals at the base of the OHC. We demonstrate in non-injected control Td/PV^{Cre} mice that the tdTomato expression is present in the HCs and afferent fibers (Figure 7A, control). At 28 dpi of AAV-DTA, tdTomato^{+} afferent fibers in both the OSL and Rosenthal's canal disappeared, while a thinner population of $TUJ1^{+}$ nerve fibers still innervated the ISB, OSL and Rosenthal's canal (Figure 7A, Td/PV^{Cre}). The MOC terminals connected to the OHCs were present (Figure 7A, Td/PV^{Cre} insets). The substantial thinning of afferent fibers forming the ISB and loss of OSB were observed in the whole-mount surface preparation in the AAV-DTA injected PV^{Cre} mice (Figure 7B, PV^{Cre}). The number and size of the radial MOC terminals in the AAV-DTA-injected mice were grossly comparable to the WT mice; however, the reduction of fibers forming the ISB suggests that the efferent fibers from the LOC were reduced (Figure 7B, PV^{Cre}). To determine the origin of the surviving radial fibers, a separate cohort of mice was stained for the presence of choline acetyltransferase (ChAT), which is immunopositive in efferent fibers. In AAV-DTA-injected PV^{Cre} mice, ChAT signaling colocalized with the surviving $TUJ1^{+}$ radial fibers and ISB fibers (Figure 7C, PV^{Cre}). Thus, we conclude that AAV-DTA selectively transfects and leads to neuronal degeneration in the afferent fibers and reduction of LOC efferent fibers.

AAV-DTA injected in adult Td/PV^{Cre} does not lead to significant SGN damage

We administered AAV-hSYN-DTA in Td/PV^{Cre} mice cochlea via the PSCC in P30 adults to examine the efficacy of viral-induced neuronal loss in the mature inner ear. The cochleae were harvested and cryosectioned at 7 dpi. Contrary to the neonatal Td/PV^{Cre} mice, we did not observe significant SGN damage from AAV-DTA injection in the adult mice (Figure S2).

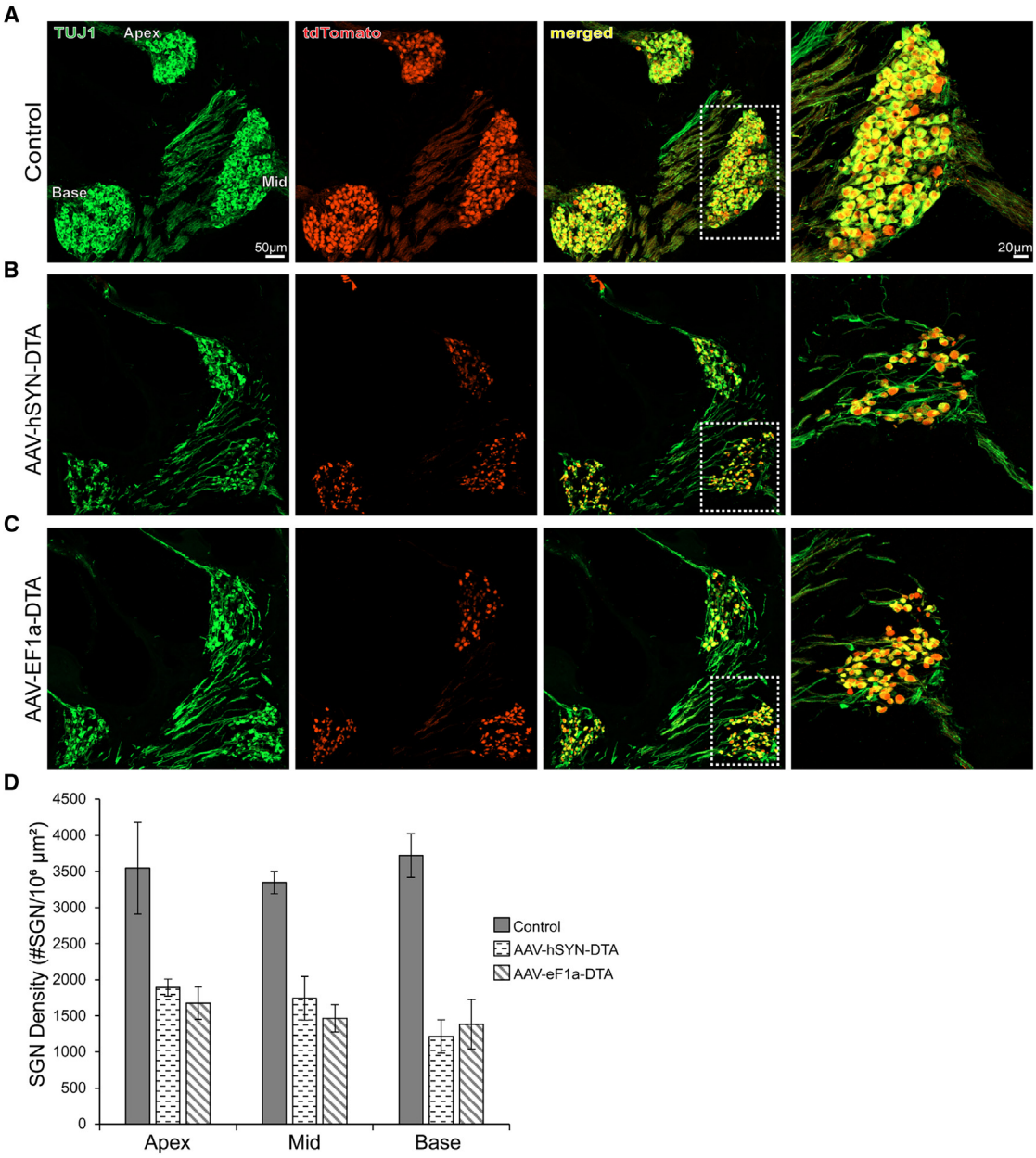

Figure 3. AAV-DTA leads to Cre-dependent SGN degeneration

After cross-breeding tdTomato/Ai9$^{+/+}$ with PV^{Cre} strain, we were able to confirm the expression of Cre recombinase in the HCs and SGN. (A) Robust tdTomato expression is observed in TUJ1^{+} SGN cells in control Td mice at P9 (n = 3). (B and C) P2 Td/PV^{Cre} mice were injected with either AAV-hSYN-DTA (n = 5) or AAV-EF1a-DTA (n = 5), both demonstrating substantial loss of both TUJ1 and tdTomato signals consistent with SGN damage. At far right, higher magnification of the respective dashed boxes in the mid-turn (A–C). (D) Quantification of SGN density showed a significant SGN degeneration of 60%–61% after 7 dpi in both AAV-hSYN-DTA- and AAV-EF1a-DTA-injected mice compared to control. No significant difference was observed between the efficacy of AAV-EF1a-DTA and AAV-hSYN-DTA in selective SGN ablation. Student's t test confirmed that there was a statistically significant degeneration of SGN in the apex, mid-, and basal turn at 7 dpi ($p < 0.05$).

DISCUSSION

In our study, we demonstrate that the SGN can be selectively ablated in neonatal PV^{Cre} mice, as evidenced by approximately 60% SGN loss within 7 days following AAV-DTA injection. At 28 dpi, the mice were profoundly deaf, while HC histology and otoacoustic emissions remained intact. Our data indicate that AAV-DTA selectively damages the SGN and causes minimal off-target damage to the HCs, consistent with AN phenotype.

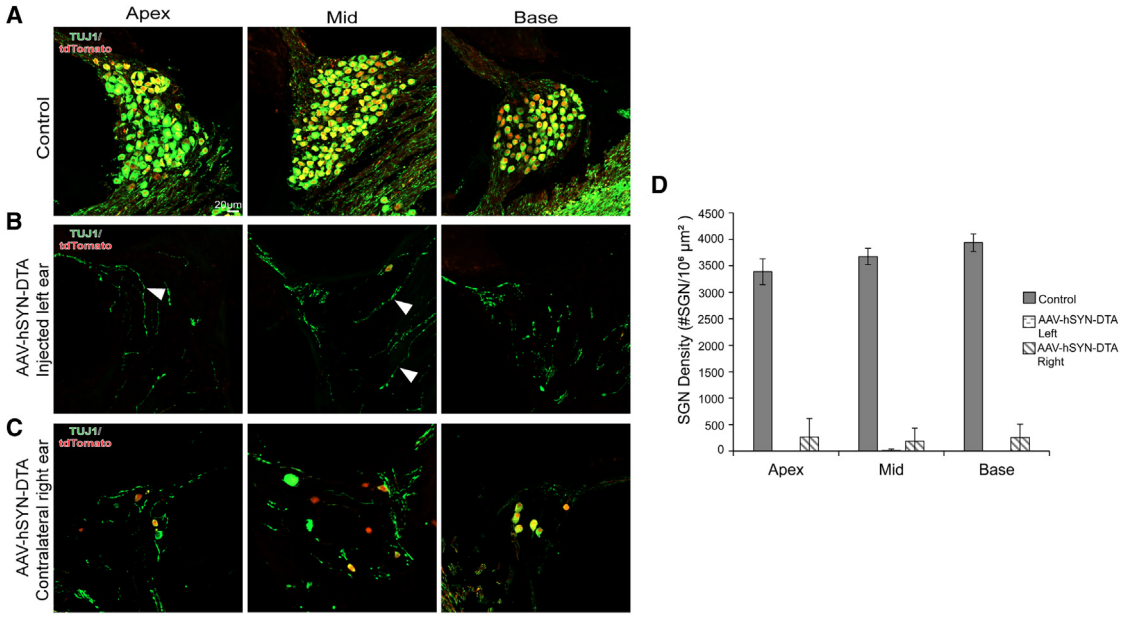

Figure 4. Time-dependent progressive degeneration of SGN

Cochleae were examined at 28 days after AAV-hSYN-DTA injections into P2 Td/PV^{Cre} mice. (A) Age-matched control Td mice in apex, mid-, and basal turns. (B) AAV-hSYN-DTA-injected Td/PV^{Cre} mice demonstrated near-total loss of SGN cells in the injected left ear. We observed crossing fibers in the Rosenthal's canal that likely represent efferent fibers (white arrowheads). (C) Contralateral ear demonstrates significant SGN damage, with few surviving SGN. (D) Quantification of SGN density showed nearly complete ablation of TUJ1 immunopositive SGN in all three turns of the injected left ear and less but significant degeneration in the contralateral right ear. In the contralateral ear, quantification of SGN density showed 92% ablation in the apex and basal turn and 94% ablation in the mid-turn ($n = 3$) ($p < 0.05$).

Ablation technique using DT is a powerful tool to examine the biological effects and function of cell-type-specific degeneration. Targeted neuronal ablation can be achieved with transgenic expression of DTR when injecting DT or by expressing DTA in cell subpopulations. Previously, groups have attempted to ablate SGN populations by generating a transgenic DTR mouse, expressing DTR in either *Bhlhb5* or *Nefl* genes that are SGN specific in the cochlea. In adult *Bhlhb5*-DTR mice, SGN loss was approximately 30%–40% at 14 dpi, which was the endpoint of the study.[15] In the *Nefl*-DTR mice, the SGN loss was 58% by 28 dpi when DT was administered at P7.[16] In our study, we achieved 60%–61% SGN ablation by 7 dpi in neonatal mice and nearly complete loss by 28 dpi of AAV-DTA into the inner ear. This discrepancy may be explained by several factors, including the age of the mouse (neonatal vs. adult), degree of Cre recombinase expression, rapid onset of DTA expression, or insufficient dosing of DT in DTR mice. Regardless, one limitation of the DTR approach is its narrow pharmacological window and potential lethal side effects, including renal and lung failure, precluding examination of DT dose-dependent studies.[33] Indeed, a previous report has shown that systematic administration of DT during the neonatal and juvenile periods in both WT C57/Bl6 and CBA mice can be ototoxic, resulting in elevated threshold shifts and significant HC and SGN damage with a single peritoneal injection of 50 μg/kg DT.[34] Therefore, selective SGN ablation in early neonatal mice using the inducible DTR model may be technically challenging.

AAV serotypes and promoters play an important role in gene delivery by inducing cell-type-specific transfection and controlling the degree of transcriptional activity. AAV2-retro is an engineered AAV variant designed to enhance neuronal tropism and retrograde tracing in the brain circuit. The specific protein insertion and point mutations (insert LADQDYTKTA + V708I + N382D) in the WT AAV2 capsid are thought to promote the binding efficacy of viral capsids to existing receptors in the AAV pathway to increase the retrograde transport of the reporter transgene along the neurons.[24,35] To our knowledge, we are the first to demonstrate the transduction profile of AAV2-retro in the inner ear. With a CMV promoter, the AAV2-retro transfects most afferent neurons without transfecting the HCs in neonatal mice (Figure 1A). The AAV2-retro demonstrates highly specific SGN affinity with minimal ectopic expression compared to other serotypes described in the literature.[36–39]

Previous reports have shown that hSYN and EF1a promoters are specific to the SGN, with little to no transfection of the HCs.[40,41] In our study, we compared the efficacy of two promoters that have selective SGN tropism and little to no transduction of the HCs with varying strengths—hSYN is neuron specific and has a moderate expression level and the EF1a promoter is an ubiquitous promoter that has the strongest expression level comparable to CAG.[41–44] We anticipated that the stronger EF1a promoter would lead to greater SGN destruction when compared to hSYN and potential HC damage. As early as 3 dpi, we observed the activation of caspase-3 followed by the release of

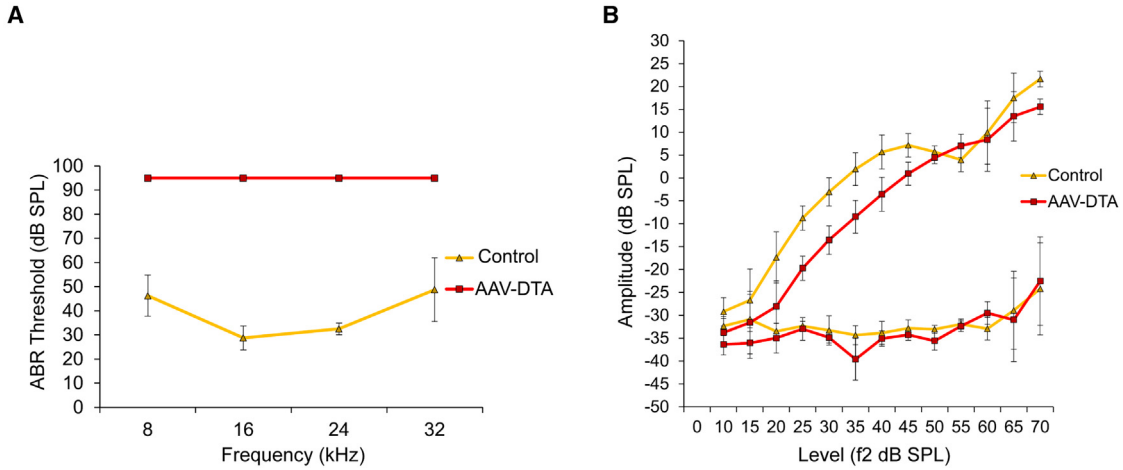

Figure 5. AAV-DTA injected mice are profoundly deaf, with elevated ABR but normal DPOAE amplitude

Functional hearing tests are performed on ≥P30 uninjected control mice and AAV-DTA 28 dpi mice (n = 3). (A) ABR showed profound hearing loss, above the 90-dB threshold, in the injected mice. (B) DPOAE showed the mean amplitude vs. level function at 16 kHz in the injected mice is comparable to controls. Our results demonstrate elevated ABR thresholds with an intact function of outer HCs (OHCs), which is consistent with auditory neuropathy.

cytochrome *c* in PV^{Cre} mice but not in WT mice following the injection of AAV-EF1a- DTA, indicating that DTA induced programmed apoptotic cell death in only targeted Cre^{+} neurons (Figures 2A and 2B). However, in our results we did not observe a significant difference in the two promoters at 1 week (EF1a 60% vs. hSYN 61%) (Figure 3). As the toxicity of DTA is potent, a single molecule of DTA is enough to kill a cell.[45,46] We speculate that because both promoters on an AAV2-retro vector transfect most afferent neurons without transducing the HCs, the expression level sufficient to promote SGN death can be achieved by moderate expression levels of the promoters. We conclude that the strength and cell specificity of the promoter do not impact the efficiency of ablation with DTA in our study. Furthermore, along with AAV-retro, we demonstrate that both hSYN and EF1a are promising candidates for optimizing gene delivery to SGNs.

FLEX is a genetic tool that allows spatiotemporal and conditional control, ultimately allowing the manipulation of specific transgenes under site-specific Cre-on or Cre-off pattern.[20,47,48] Coupling this tool with an AAV targeting a subpopulation cell type of interest in a Cre-expressing mouse line offers tighter control of transgene expression.[26,49,50] The limitations of this approach are potential off-target effects in Cre-independent cells, "leaky expression," and variable levels of Cre expression in target cells.[51,52] In our model, transgene expression of AAV-DTA followed a Cre-on pattern, in which the coding sequence of DTA is irreversibly reversed and expressed in only parvalbumin-expressing Cre^{+} cells but not in Cre^{-} cells. Likewise, the high efficiency of the AAV2-retro serotype and neuron-specific promoters to transduce SGN cells and not HCs decreases unwanted off-target effects. We anticipated that our approach would lead to minimal off-target or leaky expression of DTA in the inner ear. Furthermore, DTA released from a dying cell is unable to enter the neighboring cell cytoplasm due to the lack of DT fragment B that modulates endocytosis, thus restricting the spread of DTA.[19]

At 28 dpi, when our mice are profoundly deaf, we demonstrate the nearly complete loss of afferent neurons but preservation of HCs in all turns along with normal function represented in intact DPOAE (Figures 5 and 6). Furthermore, we observed crossing fibers without a cell body in the Rosenthal's canal area, which are consistent with efferent fibers stemming from the olivocochlear system (Figure 7A, Td/PV^{Cre}). We show that surviving radial fibers in the organ of Corti are $ChAT^{+}$, representing the MOC efferent fibers (Figure 7C, PV^{Cre}). While the MOC terminals were maintained, we observed a reduction in size and ChAT expression of the ISB in the AAV-DTA-injected mice (Figures 7B and 7C, PV^{Cre}). We speculate that the efferent fibers from the LOC, which partially constitute the ISB by connecting to the afferent fibers at the base of the IHC are diminished secondarily due to the loss of their synaptic target to the afferent fibers. Regardless, the histological evidence of the survival of both Cre^{+} HCs and partial Cre^{-} efferent fibers suggests that off-target damage to adjacent tissue in the cochlea with our approach is minimal. We conclude that our AAV-DTA approach provides selective SGN degeneration in the neonatal PV^{Cre} mouse.

We demonstrate significant neuronal damage in the non-injected contralateral right ear and vestibular ganglion neurons following the injection of 1 μL AAV-DTA into the left ear via the PSCC approach. These results indicate the diffusion of AAV-DTA to the contralateral ear and vestibule. The extent of neuronal degeneration at 28 dpi in the contralateral ear is comparable to the left ear and 85% in the vestibule, demonstrating the potency of AAV-DTA to degenerate auditory and vestibular neurons in the inner ear. In our study, we did not assess the retrograde effects of our approach as PV is expressed widely throughout the brain and in other tissues.[27,28,53] However, we did not appreciate any unusual behavioral changes or side effects in our mice following AAV-DTA injection. Further research is necessary to assess the systemic effects of

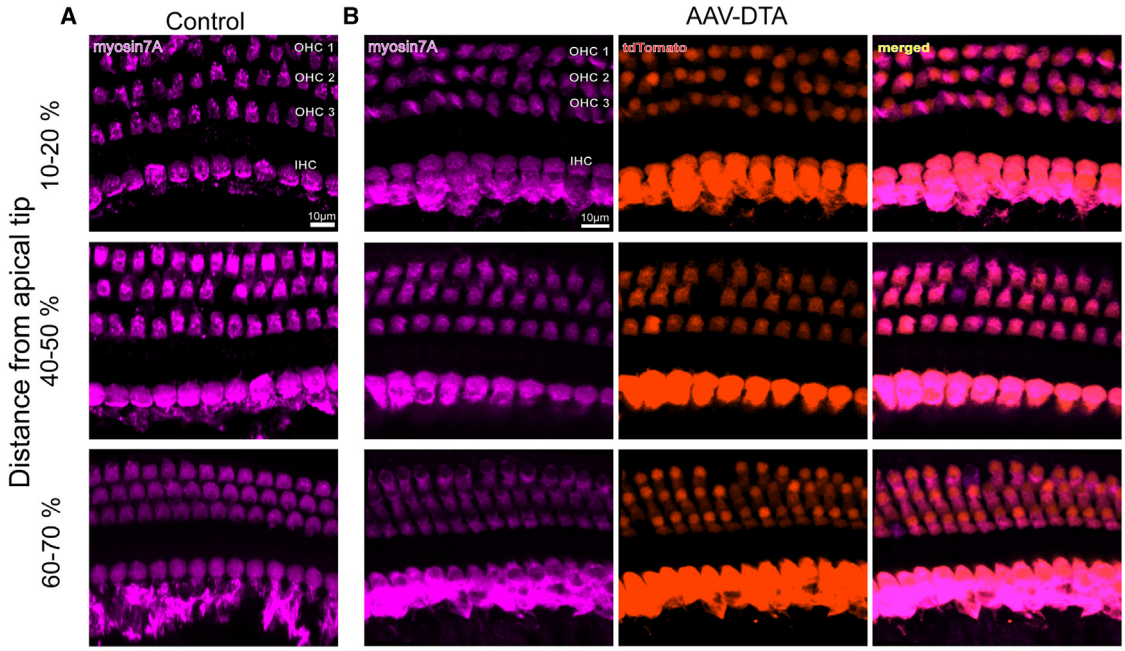

Figure 6. The morphology of the HCs remains intact

(A) We demonstrate representative whole-mount tissue at 10%–20%, 40%–50%, and 60%–70% distance from the apical tip at P30 control mice. (B) Representative whole-mount tissue at 10%–20%, 40%–50%, and 60%–70% distance from the apical tip 28 days after AAV-DTA injection in Td/PV^{Cre} mice. HCs were preserved in all turns. Colocalization of tdTomato and myo7A confirmed the expression of Cre recombinase in HCs.

AAV-DTA injected into the cochlea on the brain and other organs. While the PSCC injection approach has been reported to successfully transduce both cochlear and vestibular cells, the diffusion of viral vectors to the contralateral ear after PSCC injection has been reported previously.[54–60] One obvious pathway of AAV spread to the contralateral ear is the circulation through the cochlear aqueduct, which occurs more commonly in round window membrane injection and less commonly with PSCC injection due to the proximity of the basal turn of the cochlea to the cochlear aqueduct.[61] To prevent the diffusion of the vector to the contralateral ear, reducing the viral injection volume has been found to be effective in adult mice.[62] In future studies, we will seek to adjust the injection volume to prevent leakage to the contralateral ear in neonatal mice.

Our results demonstrate that the AAV-DTA injection did not lead to significant SGN degeneration in mature PV^{Cre} mice ($\geq$P30) in this study. The tdTomato in the Td/PV^{Cre} demonstrates that the Cre recombinase is present and stable past P30 (Figure S2). Thus, we attribute the mild degeneration pattern to the inability to effectively transduce the SGN and deliver the transgene in adult cochlea with AAV2-retro. The rate of SGN transduction is significantly lower in the adult cochlea compared to the neonatal cochlea across species.[36,63–65] For instance, AAV2/Anc80L65-CMV transduces less than 10% of the SGN population in 7-week-old mice but transduces 76% of the SGN population in neonatal mice.[66,67] While neuron-specific promoters such as hSYN may improve selective targeting of SGN, this has not been shown to improve the overall SGN transduction in adult cochlea.[65] Further modifications in AAV design, new promoters, and inner ear injection methods may contribute to the improvement in adult SGN transduction with AAV vectors.

Several important limitations remain in our study. First, because FLEX-DTA-mCherry plasmid depends on Cre-recombinase to mediate recombination and express DTA toxin in a specific cellular population, our animal model is limited to a neuronal Cre-driven strain. The development of a model that is not limited to a certain strain or Cre dependent will have greater utility and allow a broader range of genetic and molecular studies. Second, conducting a dose-dependence study by adjusting viral titers may lead to mild to moderate SGN degeneration, which may better represent the broader spectrum of the AN phenotype. Future studies are needed to address these questions.

In conclusion, the AAV-DTA viral vector successfully mediates SGN degeneration in neonatal mice, thus mimicking a severe form of AN. The rapid and specific degeneration of SGNs can accelerate future studies investigating the mechanism of SGN death and potential oto-protective strategies to attenuate neuronal loss. In addition, we achieve near-complete SGN loss, which can serve as a powerful platform to evaluate the effectiveness of regenerative approaches such as epigenetic *in situ* reprogramming and stem cell transplantation in regenerating or restoring the peripheral auditory nerve.[68,69]

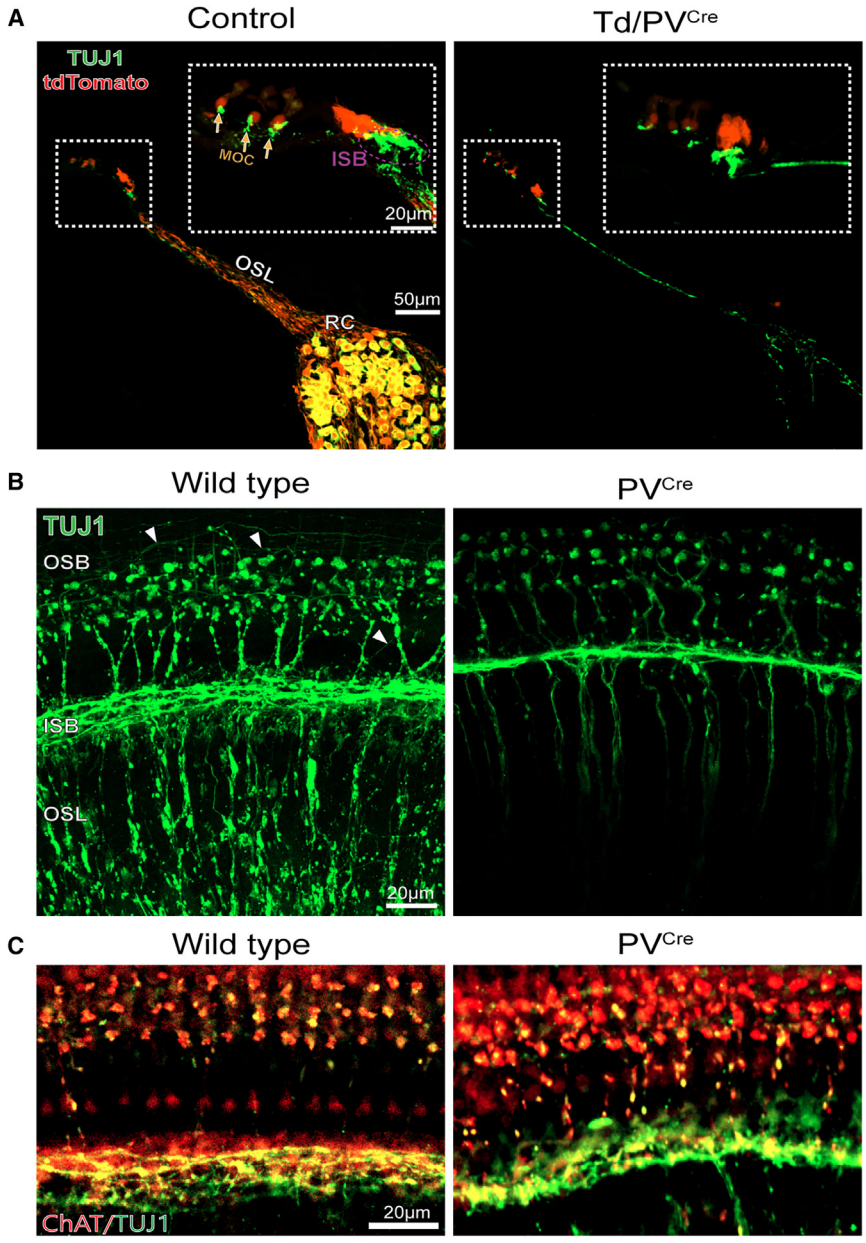

Figure 7. Afferent nerve fiber degeneration after AAV-DTA injection

(A) Representative low magnification (20×) of the mid-modiolar cochlear section of age-matched Td/PV^{Cre} control and 28 dpi Td/PV^{Cre} mice. tdTomato is expressed in the afferent fibers crossing the OSL and RC. The inserts demonstrate the magnified view of tdTomato^{+} HCs in the organ of Corti. The MOC terminal at the OHCs (yellow arrows) and ISBs (violet circle) are immunopositive for TUJ1 in the dashed box. In the AAV-DTA-injected Td/PV^{Cre} mice, the tdTomato^{+} afferent fibers are not visible while TUJ1 expression in the MOC terminal is present. (B) In adult WT whole-mount tissue, we observed the TUJ1^{+} ISB and the thin spiral fibers of type II SGN (white arrowheads) of the OSB. In the AAV-DTA-injected PV^{Cre} mice, we observed significant thinning of the ISB and neurites in the osseous spiral lamina (OSL) and near-total loss of the OSB, while the MOC terminals appear intact, but the ISB is reduced in size. (C) The efferent fibers for the olivocochlear system are immunopositive for ChAT and TUJ1 in the organ of Corti (WT). The AAV-DTA-injected PV^{Cre} mice maintain a comparable number of ChAT and TUJ1^{+} radial efferent fibers forming the MOC terminals, but the ChAT signal in the ISB is reduced compared to the WT.

MATERIALS AND METHODS

Ethics approval

The experimental procedures on animals were approved by the University of Southern California Institutional Animal Care and Use Committee (protocol no. 21248) and the Institutional Biosafety Committee (protocol no. BUA-20-00050) and were performed in accordance with the NIH Guidelines for the Care and Use of Laboratory Animals.

Animals

Pvalb-IRES-Cre or PV-Cre$^{+/+}$ (stock no. 008069), Ai9-tdTomato (stock no. 007909), and C57BL/6J (stock no. 000664) were obtained from The Jackson Laboratory (JAX). PV$^{Cre+/+}$ was bred with C57 to produce PV$^{Cre+/-}$ and with Ai9-tdTomato to produce tdTomato$^{+/-}$/PV$^{Cre+/-}$ (Td/PV^{Cre}). Mouse genotypes from tail biopsies were determined using real-time PCR with specific probes associated with corresponding JAX ID (Transnetyx).

Viral vector

AAV2-retro-EF1a-FLEX-DTA-mCherry (AAV-EF1a-DTA) and AAV2-retro-hSYN-FLEX-DTA-mCherry (AAV-hSYN-DTA) were produced by the Canadian Neurophotonics Platform Viral Vector Core , located at the CERVO Brain Research Center (RRID: SCR_016477). The viral titer was 1.2×10^{13} GC/mL. AAV-EF1a-DTA or AAV-hSYN-DTA were stored at −80°C and thawed on ice before use.

PSCC injection

Cochlear injection was performed on P1–P2 and adult mice. Before the procedure, mice were given preemptive analgesia with buprenorphine XR (3.25 mg/kg). Mice were anesthetized by inducing hypothermia. The surgery was performed on the left ear under a Leica M60 microscope. A suspension of 1,000 nL AAV-DTA was mixed with 2.5% fast green dye (Sigma-Aldrich) at a 10:1 ratio. The suspension of viral vector was loaded into a borosilicate glass capillary (World Precision Instruments) and affixed to an automated injection

system, Nanoliter 2020 injector (World Precision Instruments). A post-auricular incision exposed the sternocleidomastoid muscle. The division of the sternocleidomastoid muscle leads to the exposure of the temporal bone, facial nerve, and membranous cochlear bulla; smaller bleeding vessels are cauterized for hemostasis. Tracing the facial nerve toward the bulla would lead to identifying the lateral semicircular canal, the structure superior to the cochlear bulla. The PSCC can be subsequently identified as perpendicular to the LSCC posteriorly. The micropipette is advanced until it penetrates the PSCC, creating a canalostomy, which allows access to the perilymphatic space. Due to the relatively little ossification of PSCC at this age, PSCC can be easily pierced by the glass micropipette. In the adult mouse, the surrounding of the micropipette is sealed with Histoacryl Topical Skin Adhesive (TissueSeal, TS1050071-FP). A total volume of 1,000 nL was injected at a rate of 10 nL/s into the perilymphatic space via the PSCC canalostomy of the left ear of each mouse. The small caliber of the glass micropipette creates a small canalostomy that releases upon pipette removal; no tissue is required to seal the canalostomy to avoid leakage. Mice were closely monitored daily for at least 3 days postoperatively.

Cochlear tissue preparation

AAV-EF1a-DTA and AAV-hSYN-DTA were incubated for 7 or 28 dpi following neonatal injection. Bilateral ears were harvested after animals were euthanized by CO_2 inhalation. Temporal bones were fixed with 4% paraformaldehyde at room temperature for 2 h. The cochlea was extracted under the Leica S9i light microscope. Cochlear tissue was rinsed with 1× PBS and stored in a 4°C refrigerator. Whole-mount microdissection was performed under the light microscope. Dissected tissue was incubated with EDTA, pH 8.0, for 10 min to soften the OSL, rinsed with 1× PBS, and then infiltrated with 0.3% Triton X-100 for 10 min. Cochlear tissue was blocked with 5% normal goat serum (NGS) for 1 h. Primary antibody was diluted 1:100–500 in 1× PBS and incubated overnight in a 4°C refrigerator. Secondary antibody was diluted 1:500 in PBS and incubated for 30 min at room temperature. Rinsing with 1× PBS was performed in between stainings. For cryosection, cochlea was incubated with EDTA, pH 8.0, overnight. The cochlea could be incubated with a fresh 5 mL EDTA, pH 8.0, overnight, if necessary. Softened cochlea was rinsed with 1× PBS and then incubated with 30% sucrose solution overnight. Cochlea were then mounted in 5 × 5 × 5 cm cryomold with freezing tissue medium. Cryosection was performed with the Leica 800 Cryostat machine. The embedded tissue was sectioned parallel to the modiolus at 14 μm thickness per section. Tissue was blocked with 5% NGS for 2 h at room temperature. Both primary and secondary antibody were diluted in 5% NGS buffer. Primary staining was incubated overnight in a 4°C refrigerator, and secondary staining was incubated for 2 h at room temperature. Phalloidin 555 (A34055, Thermo Fisher Scientific) was added to secondary antibodies solution to stain for filamentous actin. Rinsing with 1× PBS was performed in between stainings. The slides were mounted with Fluoroshield mounting media.

The primary antibodies used in this study were mouse monoclonal immunoglobulin G2a (IgG2a) anti-tubulin β3 antibody (TUBB3 or TUJ1) (catalog no. 801212, BioLegend, 1:500); rabbit polyclonal IgG anti-cleaved caspase-3 (D175) antibody (catalog no. 9661, Cell Signaling Technology, 1:400); rabbit polyclonal IgG anti-cytochrome *c* antibody (catalog no. 10993-1-AP, Proteintech, 1:100); rabbit polyclonal IgG anti-myosin 7A antibody (catalog no. PA1-963, Thermo Fisher Scientific and #25-6790, Proteus Biosciences, 1:500); goat polyclonal IgG anti-chAT antibody (catalog no. AB144P, Chemicon, 1:100).

Secondary antibodies were diluted at 1:500 and they were goat anti-mouse IgG2a 488 (catalog no. A21131, Thermo Fisher Scientific), goat anti-rabbit IgG 647 (catalog no. A32733, Thermo Fisher Scientific), goat anti-rabbit IgG 555 (catalog no. A32732, Thermo Fisher Scientific), donkey anti-goat IgG 647 (catalog no. A32849, Thermo Fisher Scientific), and donkey anti-rabbit IgG 488 (catalog no. A32790, Thermo Fisher Scientific).

Cell counting and statistical analysis

Three distinct non-sequential images in the mid-modiolar region of 14-μm-thick sections were used to increase the reliability of cell density calculation at all three cochlear turns. Images of cryosection were acquired using the Leica 800 confocal microscope. Three-dimensional image areas were acquired and flattened along the z axis to obtain orthogonal views. A 20× scaled image of each turn with orthogonal view was opened with Fiji ImageJ analysis software.[70] To measure the area, Rosenthal's canal was manually selected with the "Polyclonal Selection" tool and the cross-sectional area was measured with the "Measure" option in the "Analyze" section in ImageJ. Cell counting was performed manually with the Cell Counter plugin for each fluorescent channel. Only cells exhibiting positive TUJ1 and tdTomato signals were included in SGN density calculations per 10^6 μm^2. The raw number of the cell counting was then used in the following formula to calculate the final SGN density: Raw number of cells/(Area/Conversion factor of 10^6 μm^2).

Statistical analyses of cell counting and functional hearing test were performed in Microsoft Excel. A Student t test with two tails was used to compare independent samples with equal variance. A Welch's t test with two tails was used to compare independent samples with unequal variance. Statistical significance is achieved when $p < 0.05$.

Functional hearing tests

Cochlear functional hearing was analyzed on injected mice 28 dpi and around P30–40 control mice as previously described.[71,72] The ABR test was recorded with the Eaton-Peabody Laboratories Cochlear Function Test Suite. Animals were anesthetized as described and laid on their side on a flat platform in the soundproof chamber. For ABR, three stainless-steel electrodes were placed subcutaneously under the vertex, the mastoid of the measured ear, and the thoracic region of the spine. The microphone was loosely secured in the pinna. Auditory signals were presented as tone pips with a rise and fall time of 0.5 ms and a total duration of 5 ms at frequencies 8, 16, 24, and 32 kHz. Tone pips were delivered from 10 to 90 dB, with an increase of 5 dB. Signals were presented at a rate of 30/s. Responses were filtered

with a 0.3- to 3-kHz pass-band (10,000×). For each stimulus intensity, signals were averaged over 300 repetitions. The ABR threshold was defined as the lowest sound level at which a reproducible waveform could be observed.

DPOAE protocol was followed as previously described.[73] DPOAE was measured by delivering two pure tones, f1 and f2, via a microphone placing securely in the ear canal. DPOAE was measured at 2f1–f2 with the primary frequency, f1, which was 10 dB lower than the secondary frequency, f2. The f2 frequency was set at 5.6, 8.0, 11.3, 16, 22.6, and 32 kHz, f2/f1 = 1.2. A stimulus level mode of L1 = L2 + 10 dB was used, and stimulus levels were swept in 5-dB steps from 10 to 70 dB (for f2). The amplitude of DPOAE at 2f1–f2 was extracted from the text files and graphed in Excel.

DATA AVAILABILITY

The data that support the findings of this study are available from the corresponding author upon reasonable request.

ACKNOWLEDGMENTS

This study was supported by NIH/NIDCD grant K08DC021750 (S.B.S), the AOS Clinician-Scientist Award (S.B.S), and the TRIO Career Development Grant (S.B.S). Confocal imaging was performed at the Optical Imaging Facility in the Eli and Edythe Broad Center for Regenerative Medicine. The graphical abstract was created with BioRender.com.

AUTHOR CONTRIBUTIONS

Conceptualization, S.B.S. Methodology, N.V.N., J.S.L., and S.B.S. Investigation, N.V.N., J.S.L., M.J.P., and S.B.S. Writing – original draft, N.V.N., J.S.L., M.J.P., and S.B.S. Writing – review & editing, N.V.N., J.S.L., M.J.P., and S.B.S. Funding acquisition, S.B.S. Resources, S.B.S. Supervision, S.B.S.

DECLARATION OF INTERESTS

The authors declare no competing interests.

SUPPLEMENTAL INFORMATION

Supplemental information can be found online at https://doi.org/10.1016/j.omtm.2025.101440.

REFERENCES

1. Lin, F.R., Niparko, J.K., and Ferrucci, L. (2011). Hearing Loss Prevalence in the United States. Arch. Intern. Med. *171*, 1851–1852. https://doi.org/10.1001/archinternmed.2011.506.

2. Nayagam, B.A., Muniak, M.A., and Ryugo, D.K. (2011). The spiral ganglion: connecting the peripheral and central auditory systems. Hear. Res. *278*, 2–20. https://doi.org/10.1016/j.heares.2011.04.003.

3. Carricondo, F., and Romero-Gómez, B. (2019). The Cochlear Spiral Ganglion Neurons: The Auditory Portion of the VIII Nerve. Anat. Rec. *302*, 463–471. https://doi.org/10.1002/ar.23815.

4. Liberman, M.C. (2020). Hidden hearing loss: Primary neural degeneration in the noise-damaged and aging cochlea. Acoust Sci. Technol. *41*, 59–62. https://doi.org/10.1250/ast.41.59.

5. Wu, P.Z., Liberman, L.D., Bennett, K., de Gruttola, V., O'Malley, J.T., and Liberman, M.C. (2019). Primary Neural Degeneration in the Human Cochlea: Evidence for Hidden Hearing Loss in the Aging Ear. Neuroscience *407*, 8–20. https://doi.org/10.1016/j.neuroscience.2018.07.053.

6. Stamataki, S., Francis, H.W., Lehar, M., May, B.J., and Ryugo, D.K. (2006). Synaptic alterations at inner hair cells precede spiral ganglion cell loss in aging C57BL/6J mice. Hear. Res. *221*, 104–118. https://doi.org/10.1016/j.heares.2006.07.014.

7. Sergeyenko, Y., Lall, K., Liberman, M.C., and Kujawa, S.G. (2013). Age-Related Cochlear Synaptopathy: An Early-Onset Contributor to Auditory Functional Decline. J. Neurosci. *33*, 13686–13694. https://doi.org/10.1523/JNEUROSCI.1783-13.2013.

8. Delmaghani, S., del Castillo, F.J., Michel, V., Leibovici, M., Aghaie, A., Ron, U., Van Laer, L., Ben-Tal, N., Van Camp, G., Weil, D., et al. (2006). Mutations in the gene encoding pejvakin, a newly identified protein of the afferent auditory pathway, cause DFNB59 auditory neuropathy. Nat. Genet. *38*, 770–778. https://doi.org/10.1038/ng1829.

9. De Siati, R.D., Rosenzweig, F., Gersdorff, G., Gregoire, A., Rombaux, P., and Deggouj, N. (2020). Auditory Neuropathy Spectrum Disorders: From Diagnosis to Treatment: Literature Review and Case Reports. J. Clin. Med. *9*, 1074. https://doi.org/10.3390/jcm9041074.

10. Seyyedi, M., Viana, L.M., and Nadol, J.B. (2014). Within-Subject Comparison of Word Recognition and Spiral Ganglion Cell Count in Bilateral Cochlear Implant Recipients. Otol. Neurotol. *35*, 1446–1450. https://doi.org/10.1097/MAO.0000000000000443.

11. Matsumoto, M., Sekiya, T., Kojima, K., and Ito, J. (2008). An animal experimental model of auditory neuropathy induced in rats by auditory nerve compression. Exp. Neurol. *210*, 248–256. https://doi.org/10.1016/j.expneurol.2007.11.006.

12. Schmiedt, R.A., Lang, H., Okamura, H.o., and Schulte, B.A. (2002). Effects of furosemide applied chronically to the round window: a model of metabolic presbyacusis. J. Neurosci. *22*, 9643–9650. https://doi.org/10.1523/JNEUROSCI.22-21-09643.2002.

13. Ruan, Q., Ao, H., He, J., Chen, Z., Yu, Z., Zhang, R., Wang, J., and Yin, S. (2014). Topographic and quantitative evaluation of gentamicin-induced damage to peripheral innervation of mouse cochleae. Neurotoxicology *40*, 86–96. https://doi.org/10.1016/j.neuro.2013.11.002.

14. Harrison, R.V. (1998). An animal model of auditory neuropathy. Ear Hear. *19*, 355–361. https://doi.org/10.1097/00003446-199810000-00002.

15. Pan, H., Song, Q., Huang, Y., Wang, J., Chai, R., Yin, S., and Wang, J. (2017). Auditory Neuropathy after Damage to Cochlear Spiral Ganglion Neurons in Mice Resulting from Conditional Expression of Diphtheria Toxin Receptors. Sci. Rep. *7*, 6409. https://doi.org/10.1038/s41598-017-06600-6.

16. Hu, Z., Komal, F., Singh, A., and Deng, M. (2021). Generation of a Spiral Ganglion Neuron Degeneration Mouse Model. Front. Cell Dev. Biol. *9*, 761847. https://doi.org/10.3389/fcell.2021.761847.

17. Robinson, E.A., Henriksen, O., and Maxwell, E.S. (1974). Elongation Factor 2: AMINO ACID SEQUENCE AT THE SITE OF ADENOSINE DIPHOSPHATE RIBOSYLATION. J. Biol. Chem. *249*, 5088–5093. https://doi.org/10.1016/S0021-9258(19)42331-4.

18. Van Ness, B., Howard, J.B., and Bodley, J.W. (1980). ADP-ribosylation of elongation factor 2 by diphtheria toxin. Isolation and properties of the novel ribosyl-amino acid and its hydrolysis products. J. Biol. Chem. *255*, 10717–10720. https://doi.org/10.1016/S0021-9258(19)70366-4.

19. Ruedl, C., and Jung, S. (2018). DTR-mediated conditional cell ablation-Progress and challenges. Eur. J. Immunol. *48*, 1114–1119. https://doi.org/10.1002/eji.201847527.

20. Schnütgen, F., Doerflinger, N., Calléja, C., Wendling, O., Chambon, P., and Ghyselinck, N.B. (2003). A directional strategy for monitoring Cre-mediated recombination at the cellular level in the mouse. Nat. Biotechnol. *21*, 562–565. https://doi.org/10.1038/nbt811.

21. Xu, J., and Zhu, Y. (2018). A rapid in vitro method to flip back the double-floxed inverted open reading frame in a plasmid. BMC Biotechnol. *18*, 52. https://doi.org/10.1186/s12896-018-0462-x.

22. Permyakov, E.A., and Uversky, V.N. (2022). What Is Parvalbumin for? Biomolecules *12*, 656. https://doi.org/10.3390/biom12050656.

23. Oesterle, E.C., Campbell, S., Taylor, R.R., Forge, A., and Hume, C.R. (2008). Sox2 and Jagged1 Expression in Normal and Drug-Damaged Adult Mouse Inner Ear. J. Assoc. Res. Otolaryngol. *9*, 65–89. https://doi.org/10.1007/s10162-007-0106-7.

24. Tervo, D.G.R., Hwang, B.Y., Viswanathan, S., Gaj, T., Lavzin, M., Ritola, K.D., Lindo, S., Michael, S., Kuleshova, E., Ojala, D., et al. (2016). A designer AAV variant permits efficient retrograde access to projection neurons. Neuron *92*, 372–382. https://doi.org/10.1016/j.neuron.2016.09.021.

25. Anaclet, C., De Luca, R., Venner, A., Malyshevskaya, O., Lazarus, M., Arrigoni, E., and Fuller, P.M. (2018). Genetic Activation, Inactivation, and Deletion Reveal a Limited And Nuanced Role for Somatostatin-Containing Basal Forebrain Neurons in Behavioral State Control. J. Neurosci. *38*, 5168–5181. https://doi.org/10.1523/JNEUROSCI.2955-17.2018.

26. Wu, Z., Autry, A.E., Bergan, J.F., Watabe-Uchida, M., and Dulac, C.G. (2014). Galanin neurons in the medial preoptic area govern parental behaviour. Nature *509*, 325–330. https://doi.org/10.1038/nature13307.

27. Nahar, L., Delacroix, B.M., and Nam, H.W. (2021). The Role of Parvalbumin Interneurons in Neurotransmitter Balance and Neurological Disease. Front. Psychiatr. *12*, 679960. https://doi.org/10.3389/fpsyt.2021.679960.

28. Liu, Y., Cheng He, R., Munguba, G.C., and Lee, R.K. (2023). Parvalbumin expression changes with retinal ganglion cell degeneration. Front. Neurosci. *17*, 1227116. https://doi.org/10.3389/fnins.2023.1227116.

29. Marrs, G.S., and Spirou, G.A. (2012). Embryonic assembly of auditory circuits: spiral ganglion and brainstem. J. Physiol. *590*, 2391–2408. https://doi.org/10.1113/jphysiol.2011.226886.

30. Wang, D., Tai, P.W.L., and Gao, G. (2019). Adeno-associated virus vector as a platform for gene therapy delivery. Nat. Rev. Drug Discov. *18*, 358–378. https://doi.org/10.1038/s41573-019-0012-9.

31. Huang, L.-C., Thorne, P.R., Housley, G.D., and Montgomery, J.M. (2007). Spatiotemporal definition of neurite outgrowth, refinement and retraction in the developing mouse cochlea. Dev. Camb. Engl. *134*, 2925–2933. https://doi.org/10.1242/dev.001925.

32. Goutman, J.D., Elgoyhen, A.B., and Gómez-Casati, M.E. (2015). Cochlear hair cells: The sound-sensing machines. FEBS Lett. *589*, 3354–3361. https://doi.org/10.1016/j.febslet.2015.08.030.

33. Christiaansen, A.F., Boggiatto, P.M., and Varga, S.M. (2014). Limitations of Foxp3(+) Treg depletion following viral infection in DEREG mice. J. Immunol. Methods *406*, 58–65. https://doi.org/10.1016/j.jim.2014.03.005.

34. Konishi, H., Ohgami, N., Matsushita, A., Kondo, Y., Aoyama, Y., Kobayashi, M., Nagai, T., Ugawa, S., Yamada, K., Kato, M., and Kiyama, H. (2017). Exposure to diphtheria toxin during the juvenile period impairs both inner and outer hair cells in C57BL/6 mice. Neuroscience *351*, 15–23. https://doi.org/10.1016/j.neuroscience.2017.03.028.

35. Weiss, A.R., Liguore, W.A., Domire, J.S., Button, D., and McBride, J.L. (2020). Intrastriatal AAV2.retro administration leads to extensive retrograde transport in the rhesus macaque brain: implications for disease modeling and therapeutic development. Sci. Rep. *10*, 6970. https://doi.org/10.1038/s41598-020-63559-7.

36. Shu, Y., Tao, Y., Wang, Z., Tang, Y., Li, H., Dai, P., Gao, G., and Chen, Z.-Y. (2016). Identification of Adeno-Associated Viral Vectors That Target Neonatal and Adult Mammalian Inner Ear Cell Subtypes. Hum. Gene Ther. *27*, 687–699. https://doi.org/10.1089/hum.2016.053.

37. Hu, X., Wang, J., Yao, X., Xiao, Q., Xue, Y., Wang, S., Shi, L., Shu, Y., Li, H., and Yang, H. (2019). Screened AAV variants permit efficient transduction access to supporting cells and hair cells. Cell Discov. *5*, 49. https://doi.org/10.1038/s41421-019-0115-9.

38. Landegger, L.D., Pan, B., Askew, C., Wassmer, S.J., Gluck, S.D., Galvin, A., Taylor, R., Forge, A., Stankovic, K.M., Holt, J.R., and Vandenberghe, L.H. (2017). A synthetic AAV vector enables safe and efficient gene transfer to the mammalian inner ear. Nat. Biotechnol. *35*, 280–284. https://doi.org/10.1038/nbt.3781.

39. Kang, W., Zhao, X., Sun, Z., Dong, T., Jin, C., Tong, L., Zhu, W., Tao, Y., and Wu, H. (2020). Adeno-associated virus vector enables safe and efficient Cas9 activation in neonatal and adult Cas9 knockin murine cochleae. Gene Ther. *27*, 392–405. https://doi.org/10.1038/s41434-020-0124-1.

40. Liu, Y., Okada, T., Nomoto, T., Ke, X., Kume, A., Ozawa, K., and Xiao, S. (2007). Promoter effects of adeno-associated viral vector for transgene expression in the cochlea in vivo. Exp. Mol. Med. *39*, 170–175. https://doi.org/10.1038/emm.2007.19.

41. Zhao, X., Jin, C., Dong, T., Sun, Z., Zheng, X., Feng, B., Cheng, Z., Li, X., Tao, Y., and Wu, H. (2020). Characterization of promoters for adeno-associated virus mediated efficient Cas9 activation in adult Cas9 knock-in murine cochleae. Hear. Res. *394*, 107999. https://doi.org/10.1016/j.heares.2020.107999.

42. Nieuwenhuis, B., Laperrousaz, E., Tribble, J.R., Verhaagen, J., Fawcett, J.W., Martin, K.R., Williams, P.A., and Osborne, A. (2023). Improving adeno-associated viral (AAV) vector-mediated transgene expression in retinal ganglion cells: comparison of five promoters. Gene Ther. *30*, 503–519. https://doi.org/10.1038/s41434-022-00380-z.

43. Teschendorf, C., Warrington, K.H., Siemann, D.W., and Muzyczka, N. (2002). Comparison of the EF-1 alpha and the CMV promoter for engineering stable tumor cell lines using recombinant adeno-associated virus. Anticancer Res. *22*, 3325–3330.

44. Mizushima, S., and Nagata, S. (1990). pEF-BOS, a powerful mammalian expression vector. Nucleic Acids Res. *18*, 5322.

45. Brockschnieder, D., Lappe-Siefke, C., Goebbels, S., Boesl, M.R., Nave, K.-A., and Riethmacher, D. (2004). Cell depletion due to diphtheria toxin fragment A after Cre-mediated recombination. Mol. Cell Biol. *24*, 7636–7642. https://doi.org/10.1128/MCB.24.17.7636-7642.2004.

46. Brockschnieder, D., Pechmann, Y., Sonnenberg-Riethmacher, E., and Riethmacher, D. (2006). An improved mouse line for Cre-induced cell ablation due to diphtheria toxin A, expressed from the Rosa26 locus. Genesis *44*, 322–327. https://doi.org/10.1002/dvg.20218.

47. Atasoy, D., Aponte, Y., Su, H.H., and Sternson, S.M. (2008). A FLEX switch targets Channelrhodopsin-2 to multiple cell types for imaging and long-range circuit mapping. J. Neurosci. *28*, 7025–7030. https://doi.org/10.1523/JNEUROSCI.1954-08.2008.

48. Saunders, A., Johnson, C.A., and Sabatini, B.L. (2012). Novel recombinant adeno-associated viruses for Cre activated and inactivated transgene expression in neurons. Front. Neural Circ. *6*, 47. https://doi.org/10.3389/fncir.2012.00047.

49. Foster, E., Wildner, H., Tudeau, L., Haueter, S., Ralvenius, W.T., Jegen, M., Johannssen, H., Hösli, L., Haenraets, K., Ghanem, A., et al. (2015). Targeted ablation, silencing, and activation establish glycinergic dorsal horn neurons as key components of a spinal gate for pain and itch. Neuron *85*, 1289–1304. https://doi.org/10.1016/j.neuron.2015.02.028.

50. Duarte Azevedo, M., Sander, S., Jeanneret, C., Olfat, S., and Tenenbaum, L. (2021). Selective targeting of striatal parvalbumin-expressing interneurons for transgene delivery. J. Neurosci. Methods *354*, 109105. https://doi.org/10.1016/j.jneumeth.2021.109105.

51. Saunders, A., Huang, K.W., and Sabatini, B.L. (2016). Globus Pallidus Externus Neurons Expressing parvalbumin Interconnect the Subthalamic Nucleus and Striatal Interneurons. PLoS One *11*, e0149798. https://doi.org/10.1371/journal.pone.0149798.

52. Fischer, K.B., Collins, H.K., and Callaway, E.M. (2019). Sources of off-target expression from recombinase-dependent AAV vectors and mitigation with cross-over insensitive ATG-out vectors. Proc. Natl. Acad. Sci. USA *116*, 27001–27010. https://doi.org/10.1073/pnas.1915974116.

53. Kobayashi, Y., and Hensch, T.K. (2013). Germline recombination by conditional gene targeting with Parvalbumin-Cre lines. Front. Neural Circ. *7*, 168. https://doi.org/10.3389/fncir.2013.00168.

54. Okada, H., Iizuka, T., Mochizuki, H., Nihira, T., Kamiya, K., Inoshita, A., Kasagi, H., Kasai, M., and Ikeda, K. (2012). Gene transfer targeting mouse vestibule using adenovirus and adeno-associated virus vectors. Otol. Neurotol. *33*, 655–659. https://doi.org/10.1097/MAO.0b013e31825368d1.

55. Isgrig, K., Shteamer, J.W., Belyantseva, I.A., Drummond, M.C., Fitzgerald, T.S., Vijayakumar, S., Jones, S.M., Griffith, A.J., Friedman, T.B., Cunningham, L.L., and Chien, W.W. (2017). Gene Therapy Restores Balance and Auditory Functions in a Mouse Model of Usher Syndrome. Mol. Ther. *25*, 780–791. https://doi.org/10.1016/j.ymthe.2017.01.007.

56. Wu, X., Zhang, L., Li, Y., Zhang, W., Wang, J., Cai, C., and Lin, X. (2021). Gene therapy via canalostomy approach preserves auditory and vestibular functions in a mouse model of Jervell and Lange-Nielsen syndrome type 2. Nat. Commun. *12*, 697. https://doi.org/10.1038/s41467-020-20808-7.

57. Lalwani, A.K., Han, J.J., Walsh, B.J., Zolotukhin, S., Muzyczka, N., and Mhatre, A.N. (1997). Green fluorescent protein as a reporter for gene transfer studies in the cochlea. Hear. Res. *114*, 139–147. https://doi.org/10.1016/S0378-5955(97)00151-2.

58. Lalwani, A.K., Walsh, B.J., Carvalho, G.J., Muzyczka, N., and Mhatre, A.N. (1998). Expression of adeno-associated virus integrated transgene within the mammalian vestibular organs. Am. J. Otol. *19*, 390–395.

59. Stöver, T., Yagi, M., and Raphael, Y. (2000). Transduction of the contralateral ear after adenovirus-mediated cochlear gene transfer. Gene Ther. *7*, 377–383. https://doi.org/10.1038/sj.gt.3301108.

60. Staecker, H., Bert, W., O'Malley, J., O'Malley, B.W., Jr., and Van De Water, T.R. (2001). Gene Expression in the Mammalian Cochlea: A Study of Multiple Vector Systems. Acta Otolaryngol. *121*, 157–163. https://doi.org/10.1080/00016480130 0043307.

61. Talaei, S., Schnee, M.E., Aaron, K.A., and Ricci, A.J. (2019). Dye Tracking Following Posterior Semicircular Canal or Round Window Membrane Injections Suggests a Role for the Cochlea Aqueduct in Modulating Distribution. Front. Cell. Neurosci. *13*, 471. https://doi.org/10.3389/fncel.2019.00471.

62. Kawamoto, K., Oh, S.H., Kanzaki, S., Brown, N., and Raphael, Y. (2001). The functional and structural outcome of inner ear gene transfer via the vestibular and cochlear fluids in mice. Mol. Ther. *4*, 575–585. https://doi.org/10.1006/mthe.2001.0490.

63. Zheng, H., Qiao, C., Wang, C.-H., Li, J., Li, J., Yuan, Z., Zhang, C., and Xiao, X. (2010). Efficient retrograde transport of adeno-associated virus type 8 to spinal cord and dorsal root ganglion after vector delivery in muscle. Hum. Gene Ther. *21*, 87–97. https://doi.org/10.1089/hum.2009.131.

64. Yang, O.J., Robilotto, G.L., Alom, F., Alemán, K., Devulapally, K., Morris, A., and Mickle, A.D. (2023). Evaluating the transduction efficiency of systemically delivered AAV vectors in the rat nervous system. Front. Neurosci. *17*, 1001007. https://doi.org/10.3389/fnins.2023.1001007.

65. Huet, A.T., Dombrowski, T., Rankovic, V., Thirumalai, A., and Moser, T. (2021). Developing Fast, Red-Light Optogenetic Stimulation of Spiral Ganglion Neurons for Future Optical Cochlear Implants. Front. Mol. Neurosci. *14*, 635897. https://doi.org/10.3389/fnmol.2021.635897.

66. Suzuki, J., Hashimoto, K., Xiao, R., Vandenberghe, L.H., and Liberman, M.C. (2017). Cochlear gene therapy with ancestral AAV in adult mice: complete transduction of inner hair cells without cochlear dysfunction. Sci. Rep. *7*, 45524. https://doi.org/10.1038/srep45524.

67. Duarte, M.J., Kanumuri, V.V., Landegger, L.D., Tarabichi, O., Sinha, S., Meng, X., Hight, A.E., Kozin, E.D., Stankovic, K.M., Brown, M.C., and Lee, D.J. (2018). Ancestral Adeno-Associated Virus Vector Delivery of Opsins to Spiral Ganglion Neurons: Implications for Optogenetic Cochlear Implants. Mol. Ther. *26*, 1931–1939. https://doi.org/10.1016/j.ymthe.2018.05.023.

68. Meas, S.J., Zhang, C.-L., and Dabdoub, A. (2018). Reprogramming Glia Into Neurons in the Peripheral Auditory System as a Solution for Sensorineural Hearing Loss: Lessons From the Central Nervous System. Front. Mol. Neurosci. *11*, 77. https://doi.org/10.3389/fnmol.2018.00077.

69. Wang, M., Xu, L., Han, Y., Wang, X., Chen, F., Lu, J., Wang, H., and Liu, W. (2021). Regulation of Spiral Ganglion Neuron Regeneration as a Therapeutic Strategy in Sensorineural Hearing Loss. Front. Mol. Neurosci. *14*, 829564. https://doi.org/10.3389/fnmol.2021.829564.

70. Schneider, C.A., Rasband, W.S., and Eliceiri, K.W. (2012). NIH Image to ImageJ: 25 years of image analysis. Nat. Methods *9*, 671–675. https://doi.org/10.1038/nmeth.2089.

71. Salehi, P., Ge, M.X., Gundimeda, U., Michelle Baum, L., Lael Cantu, H., Lavinsky, J., Tao, L., Myint, A., Cruz, C., Wang, J., et al. (2017). Role of Neuropilin-1/Semaphorin-3A signaling in the functional and morphological integrity of the cochlea. PLoS Genet. *13*, e1007048. https://doi.org/10.1371/journal.pgen.1007048.

72. Cutri, R.M., Lin, J., Nguyen, N.V., Shakya, D., and Shibata, S.B. (2023). Neomycin-induced deafness in neonatal mice. J. Neurosci. Methods *391*, 109852. https://doi.org/10.1016/j.jneumeth.2023.109852.

73. Maison, S.F., Liu, X.-P., Vetter, D.E., Eatock, R.A., Nathanson, N.M., Wess, J., and Liberman, M.C. (2010). Muscarinic Signaling in the Cochlea: Presynaptic and Postsynaptic Effects on Efferent Feedback and Afferent Excitability. J. Neurosci. *30*, 6751–6762. https://doi.org/10.1523/JNEUROSCI.5080-09.2010.